Gas phase photofuel cell consisting of WO_3- and TiO_2-photoanodes and an air-exposed cathode for simultaneous air purification and electricity generation

Myrthe Van Hal[1,3], Rui Campos[2,3], Silvia Lenaerts[1,3], Karolien De Wael[2,3], Sammy W. Verbruggen[1,3*]

[1] Sustainable Energy, Air & Water Technology (DuEL), Department of Bioscience Engineering, University of Antwerp, Groenenborgerlaan 171, 2020 Antwerp, Belgium

[2] Antwerp X-ray analysis, Electrochemistry and Speciation (AXES), Department of Bioscience Engineering, University of Antwerp, Groenenborgerlaan 171, 2020 Antwerp, Belgium

[3] NANOlab Center of Excellence, Groenenborgerlaan 171, 2020 Antwerp, Belgium

* Corresponding author. E-mail address: Sammy.verbruggen@uantwerpen.be

Abstract

Research has shown the potential of photofuel cells (PFCs) for waste water treatment, enabling the (partial) recovery of the energy released from the degraded compounds as electricity. Literature on PFCs targeting air pollution on the other hand is extremely scarce. In this work an autonomously operating air purification device targeting sustainable electricity generation is presented. Knowledge on gas phase operation of PFCs was gathered by combining photocatalytic and photoelectrochemical measurements, both for TiO_2 and WO_3-based photocatalysts. While TiO_2-based photocatalysts performed better in direct photocatalytic experiments, they were outperformed by WO_3-based photoanodes in all-gas-phase PFC operation. Not only do WO_3-based photocatalysts generate the highest steady state photocurrent, they also achieved the highest fuel-to-electricity conversion (> 65%). The discrepancies between gas phase photocatalytic and photoelectrochemical processes highlight the difference in driving material properties. This study serves as a proof-of-concept towards development of an autonomous, low-cost and widely applicable waste gas-to-electricity PFC device.

Keywords

Air purification, photocatalysis, photoelectrochemistry, photofuel cell, WO_3, TiO2, methanol, gas phase

1. Introduction

Air pollution is a global environmental issue that affects human health [1]. Heterogeneous photocatalysis has since long been identified as a possible solution, using light to produce electron-hole pairs that can be used in oxidation/reduction reactions of harmful compounds [2,3]. More specifically, systems using photocatalytically generated electron-hole pairs to promote electrochemical reactions (*e.g.* light-driven energy storage systems) are currently an important area of study [4–6]. In this study a photoelectrochemical (PEC) cell will be investigated, generally applying photocatalytic reactions at the anode and electrochemical H_2 production at the cathode. PEC devices have shown promising results for treating waste streams with simultaneous energy recovery [7], addressing in a single device the quest for environmental sanitation and more sustainable energy production. Most of the research on PEC technology targets waste water treatment [7–12], however, recently PEC cells targeting H_2 production applied in gas phase also turned out to be promising [13–17]. Indeed, a study by Verbruggen and co-workers showed that 30% higher photocurrents were obtained when a vapour feed was fed to the cell instead of the pure liquid feed [17]. However, when targeting simultaneous energy recovery, several bottlenecks are associated with PEC cells targeting H_2 production. Due to the redox potential of H_2 evolution, an external bias is almost always required for steady operation, thus reducing the net energy gain such a cell can provide. In addition, further H_2-processing infrastructure is required to handle the evolved H_2 gas, while only very small amounts of H_2 can be produced by an autonomous device [18]. As an alternative approach, in 2006 Kaneko presented a photofuel cell (PFC) [19], which is basically a PEC cell with an O_2-reducing cathode, degrading waste products and pollutants acting as the fuel at the anode, while simultaneously recovering part of the energy stored in these compounds as electricity.

While PFCs running on liquid feeds have since become an increasingly studied research area, research on PEC technology using a gas feed and targeting electricity generation (*i.e.* gas phase PFC) is extremely rare, with only a single paper reporting on this topic so far, in which just one type of TiO_2-based

photoanode is considered [20]. In the present work, an all-solid PEC cell built around a membrane electrode assembly (MEA) is used, based on the initial concept of a two-compartment 'reverse fuel cell' as first proposed by Seger and Kamat in 2009 [21]. Five either TiO_2- or WO_3-based photocatalysts were studied, both from commercially available sources (P25, PC500 and WO_3 nanoparticles) and prepared through established protocols ($TiO_{2\ Qiu}$ and $WO_{3\ Mart.}$), this way covering a broad range of material properties. In literature, methanol is broadly used as a model VOC and is therefore also used in this study. As photocatalysis is the driving force behind the reactions at the photoanode, and consequently the entire cell operation, the first part of this study focusses purely on the photocatalytic behaviour. In the second part of this study, chronoamperometry (CA) and cyclic voltammetry (CV) measurements were combined to characterise the all-gas phase PFC system in more detail.

The goal of this study is to showcase the potential of a robust, autonomous, low-cost and widely applicable PFC device for waste gas-to-electricity conversion. By doing so, the key performance indicators of the studied PFC systems - unconventionally operated entirely in gas phase - are obtained. The comparison with a direct photocatalytic process enables the identification of the different driving material properties in both processes.

2. Experimental

2.1. Material synthesis and characterisation

Five different photocatalysts were studied: commercially available P25 (Evonik), WO_3 nanopowder (Sigma-Aldrich) and PC500 (CristalACTiV), and photocatalysts synthesized according to established protocols: TiO_2 according to Qiu *et al.* (2006) [22] and WO_3 after Martínez-de la Cruz *et al.* (2010) [23] further denoted as $TiO_{2\ Qiu}$ and $WO_{3\ Mart.}$ respectively. This set of five materials provides a broad range of varying material properties (surface area, band gap, electronic properties, crystalline composition). Since we rely on materials of which the synthesis and characterisation have already been established

in literature, only a brief layout on the synthesis procedures, and basic characterisation results that validate the syntheses, can be retrieved from the Supporting Information section (materials synthesis, characterisation, or catalyst optimisation is outside the scope of this study).

2.2. Photocatalytic measurements

As the photocatalytic reactions occurring at the photoanode of a PFC initiate all further reactions occurring in the PFC system, the photoactive properties of the anode material are crucial for PFC performance and will be studied as such in this first part. Therefore, a custom-made slit-shaped photocatalytic reactor, sealed with a quartz glass on top, with an internal reactor volume of 150 mm x 20 mm x 2.75 mm was used for screening the different photocatalytic materials. A schematic illustration of the entire setup and reactor geometry is available in earlier work [24]. The samples were coated on glass slides and placed in the middle of the reactor bed. First, soda lime glass slides (25 mm x 15 mm, VWR) were washed in Piranha solution (70% sulfuric acid (H_2SO_4, Chem-Lab), 30% hydrogen peroxide (H_2O_2, ChemLab)) for 30 minutes. Application of the coating was performed by drop casting the suspension (the photocatalytic materials were suspended in methanol (Merck) by sonication for 1 hour (16.7 mg mL^{-1})) on a dry glass slide, resulting in a photocatalyst coverage of 0.9 mg cm^{-2}. The glass slides were then dried in air at room temperature for 2 hours and subsequently overnight at 90°C. Next, the glass slides were placed in a vacuum oven at 35°C for 2 hours and were finally illuminated with UVA for 6 hours in the flat plate reactor under constant flushing (2 L N_2 min^{-1}, Messer) to remove all remaining traces of organic solvent. For each photocatalytic gas phase experiment, six coated glass slides were used.

For the actual photocatalytic test, air (composed of 720 mL N_2 min^{-1} and 190 mL O_2 min^{-1} (Messer)) was bubbled through a gas wash bottle containing an aqueous 5 wt% methanol solution before entering the photocatalytic reactor, resulting in a moist methanol vapour with a methanol vapour concentration

of 28 mmol m^{-3}. To reach an adsorption/desorption equilibrium the reactor was closed for 2 hours and subsequently illuminated using a Philips Cleo UVA lamp (25 W) placed longitudinally over the sample area at a distance of 1 cm resulting in an incident intensity of 4.25 mW cm^{-2} with a maximum emission around 370 nm (confirmed using an Avantes AvaSpec-3648 spectrometer). After 24 h of continuous illumination, the reactor was purged with pure nitrogen gas (200 mL min^{-1}) and the composition of the reactor outlet was monitored in-line by FTIR spectroscopy (Thermo Fisher Scientific Nicolet 380 with ZnSe windows and 2 m heated gas cell). A dark control experiment (same setup, 24 h in dark) was performed before each light measurement to account for any intrinsic activity and potential minor leakage. Macros Basic software was used to determine the amount of methanol and CO_2 present in the outlet flow after 24 h of reaction. To that end the C-O stretching vibration bands of methanol (at 1034 cm^{-1}, $\nu_{C\text{-}O}$) and the O=C=O asymmetrical stretching vibration bands of CO_2 (at 2360 cm^{-1}, $\nu_{as\ O=C=O}$) were recorded over time. These spectral features were selected as they do not interfere with any other species present in the gas mixture. To obtain the conversion efficiency (Eq. 1) the amount of methanol present in the outlet flow was expressed as the integrated surface under the IR band (S), both for the dark and light measurement.

$$Conversion\ efficiency\ (\%) = \frac{S_{dark} - S_{light}}{S_{dark}} \times 100 \qquad \text{(Eq. 1)}$$

2.3. Photoelectrochemical measurements

An in-house engineered PFC (50 mm x 50 mm x 30 mm, Figure 1) was used for all electrochemical measurements. To obtain an economically viable, competitive technology, a low-cost robust cell design is required. Therefore, for this study an inexpensive PFC was designed mainly consisting of chemically resistant poly(methyl methacrylate) (PMMA). The inlet and outlet flow are divided over six different channels (respectively 1.2, 1, 0.8, 0.8, 1 and 1.2 mm internal diameter), that result in a steady laminar flow pattern, as illustrated in the Supporting Information section (Fig. S1). A quartz window (13 mm x

13 mm) covers the photoanode to allow UV transparency. The PFC can be used in a two- and a three-electrode configuration. By default, it is equipped with two stainless steel wires, and an additional platinum wire can be added as working electrode at the photoanode of the three-electrode cell to allow voltammetry measurements (Fig. S2).

For preparing the photoanode, the photocatalyst was suspended in an isopropanol solution (containing 3 wt% Nafion, Fuel Cell Earth) and drop casted on Toray carbon paper 030 (Fuel Cell Earth), resulting in a photocatalyst loading of 1.6 mg cm^{-2}. For the cathode, platinum nanoparticles on carbon black (10 wt% Pt, Pt-C, Sigma-Aldrich) were suspended in an isopropanol solution (incl. 3 wt% Nafion) and drop casted on Toray carbon paper 030 resulting in a loading of 0.4 mg Pt-C cm^{-2}. Both anode and cathode were dried overnight at 80°C. A membrane electrode assembly (MEA) was achieved by hot-pressing (5.5 tons and 135°C for 3 min) both anode and cathode on opposite sides of a preconditioned Nafion 117 membrane (Fuel Cell Earth) after adding 12 µL Nafion solution (5 wt%, Fuel Cell Earth) on the anode. Before use, the MEA was illuminated with UV light (Philips Cleo, 25 W), in humid atmosphere, for two days to remove residual traces of solvent. The MEA was subsequently sandwiched between the anode and cathode side of the PFC. A Philips fluorescence S 25 W UVA lamp was positioned 3 cm from the photoanode of the PFC. This resulted in an incident intensity of 2.35 mW cm^{-2} at the photoanode (max. emission at 353 nm). The complete PFC setup as used in this study is schematically shown in the Supporting Information section (Fig. S3). Additional experiments were performed using a 300 W Xe source (Oriel Instruments), equipped with an AM1.5 filter to provide simulated solar light adjusted at a total irradiance of 100 mW cm^{-2} (between 300 and 1100 nm). For visible light experiments, a 420 nm cut-on filter was added. The absolute irradiance spectrum of all used lamps can be obtained from the Supporting Information section (Fig. S4).

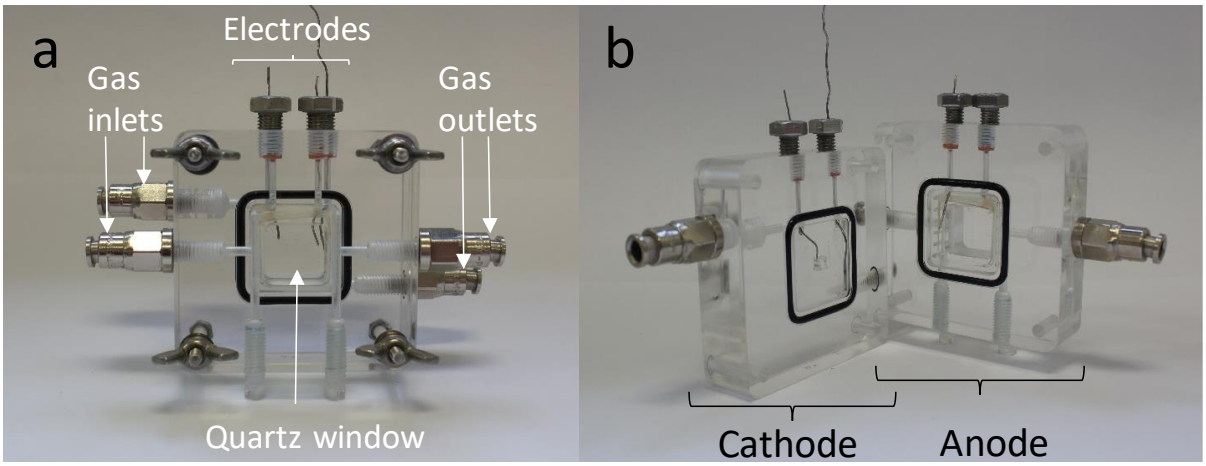

Figure 1. Three-electrode PFC employed in this study when a) closed and b) open.

A fully automated, modular test gas setup was used to conduct the gas phase experiments. Using a gas wash bottle mounted in the gas setup, methanol and water vapour are introduced at the anode. Synthetic air (21 % O_2 in N_2 (Messer)) as carrier gas was sent through the gas wash bottle and fed to the anode inlet at a flow rate of 50 mL min^{-1}. The cathode was not flushed as the final goal is to enable autonomous operation of the PFC (*e.g.* using sunlight, unbiased and without active flushing of the cathode). All CA and CV measurements were performed using a VersaSTAT 3 potentiostat (Princeton Applied Research). Before each methanol measurement the PFC was flushed with the moist methanol vapour to reach equilibrium (stable photocurrent and IR signal). For the unbiased CA measurements, the photoanode was first illuminated for 6 min, followed by 6 min in dark and finally 20 min of UV illumination while constantly flushing the photoanode with moist methanol vapour. Six different methanol concentrations were studied, corresponding to solutions containing 0, 0.1, 0.5, 1, 3 and 5 wt% of methanol in water, eventually resulting in moist methanol vapours with concentrations of respectively 0, 0.6, 2.8, 5.6, 16.9 and 28.1 mmol m^{-3} in air (0, 86, 429, 858, 2573 and 4288 ppmv), respectively. CV was performed for all studied photocatalysts for a methanol concentration of 17 mmol m^{-3} at 10 mV s^{-1} both in dark and under UV illumination. The system was allowed to equilibrate for 5 s at the starting potential prior to each measurement. Each measurement consisted

of three cycles in dark and three under UV illumination. The third cycle of each experiment was used for analysis.

3. Results and discussion

3.1. Characterisation of the photocatalysts

The five photocatalysts selected for this study (P25, $TiO_{2\ Qiu}$, $WO_{3\ Sigma}$, $WO_{3\ Mart.}$ and PC500) have already been extensively described in literature or by the manufacturer [22,25]. To confirm correct synthesis of the two photocatalysts prepared in the lab, several standard physico-chemical characterisation experiments (N_2 sorption, UV-VIS spectroscopy, X-ray diffraction and energy dispersive X-ray fluorescence) were performed. An overview of relevant photocatalyst properties is shown in Table 1, highlighting the variety in material characteristics that are covered by the different selected photocatalysts. A more detailed characterisation of the studied photocatalysts, including N_2 sorption isotherms, XRD patterns and XRF spectra, can be found in the Supporting Information section. Please note that material optimisation is outside the scope of this study.

Table 1. Physical characteristics (bandgap, BET surface area and crystallite particle size) of commercial and synthesized materials.

Material	Bandgap Eg (eV)[3]	Surface area BET ($m^2\ g^{-1}$)	Crystallite particle size (nm)[4]
$P25_{Evonik}$[1]	3.2	52	19 (A)[5], 32 (R)[5]
$TiO_{2\ Qiu}$[2]	3.1	68	30 (A)[5], 36 (R)[5]
$WO_{3\ Sigma}$[1]	2.6	7	< 100[6]
$WO_{3\ Mart.}$[2]	2.6	9	17
$PC500_{CristalACTiV}$[1]	3.3	295	9.5[7]

1) Commercially available photocatalysts.
2) Photocatalysts synthesized based on literature protocols.
3) Obtained by the Tauc method applied on diffuse reflectance spectra.
4) Estimated from XRD using the Scherrer equation.
5) A= anatase, R=rutile.
6) According to manufacturer data (Sigma-Aldrich).
7) According to data obtained by Nuño and co-workers in 2016 [26].

3.2. Photocatalytic measurements

In a PFC, the photocatalytic reactions occurring at the photoanode are the driving force behind all further reactions, so obtaining a better understanding of gas phase PFC operation implies proper knowledge on the photocatalytic reactions that lie at the base of the PFC operation. In order to do so, the first part of this study focuses on the purely photocatalytic degradation of moist methanol vapour by the five selected photocatalysts.

The reaction products (both gaseous and adsorbed on the substrate) were determined by FTIR. After 24 h of reaction (both under UV illumination and in dark) the content of the slit-shaped reactor was sent to a FTIR spectrometer. The IR spectra are shown in the Supporting Information section (Fig. S8). Besides CO, CO_2, H_2O and methanol no other stable gaseous intermediates were observed in detectable amounts in the spectra obtained after 24 h UV illumination, pointing at the almost complete oxidation of methanol to CO_2, with formation of small amounts of CO as by-product (not observed for P25). The photocatalytic performance of the different photocatalysts towards methanol degradation, and thus complete conversion to CO_2, was assessed by the ratios of methanol and CO_2 before and after illumination. Figure S9 in Supporting Information illustrates the differences in methanol-to-CO_2 conversion under dark *vs*. UV-irradiation, as derived from the areas under the FTIR absorbance *vs*. time plots obtained by flushing the resulting reaction mixture after 24 h of reaction. As expected, for all studied photocatalysts a decrease in the amount of methanol and an increase in the amount of CO_2 can be observed after illumination of the samples.

Figure 2 shows that all selected materials present significant methanol conversion (> 64%), with the highest conversion being obtained by $TiO_{2\ Qiu,\ 2006}$ (87%), followed by PC500 (78%), P25 (76%), while both WO_3-based materials exhibit a slightly lower methanol conversion around 65%. The very small surface area (< 10 $m^2\ g^{-1}$) of both WO_3-based materials can already in part explain their lower methanol conversion efficiencies [27]. Crystal structure and present crystal facets are known to influence photocatalytic methanol oxidation, both due to the effect of ions coordination and the type of adsorption of water and methanol on the photocatalyst surface [28]. Although anatase is known to be

more active than rutile, the combination of anatase and rutile, as present in both P25 and $TiO_{2\ Qiu}$, might result in a higher conversion efficiency due to synergistic effects that can be ascribed to enhanced charge separation between the anatase and rutile phases [29]. In addition, faster electron-hole recombination in smaller particles could contribute to the lower methanol conversion presented by P25 and PC500 when compared to $TiO_{2\ Qiu}$ [27]. An additional asset of $TiO_{2\ Qiu}$, is its favourable mesoporous structure (Table 1) compared to the other studied photocatalysts. Toledo and co-workers compared pure P25 with a P25-WO_3 photocatalyst and showed that under UV illumination the addition of WO_3 led to a decrease in photocatalytic hydrogen production, which is related to lower methanol conversion. Under UV illumination, TiO_2 outperformed WO_3 for photocatalytic methanol conversion, as is also evidenced in this study. On the other hand, WO_3 can, in contrast to TiO_2, use part of the visible light spectrum and that makes it a promising material for use in sunlight-driven (autonomous) applications, but is not considered here [30].

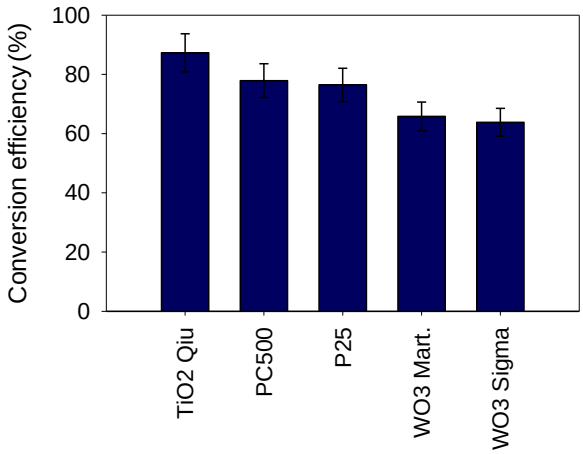

Figure 2. Photocatalytic test results using the slit-shaped reactor: methanol conversion efficiencies of all studied photocatalysts.

3.3. Photoelectrochemical measurements

The combination of unbiased CA with CV measurements (broad potential windows) for the five selected photocatalysts increases the limited knowledge on gas phase PFC operation towards simultaneous waste gas degradation and electricity production. Coupled with results of the photocatalytic methanol oxidation, this will enable the identification of crucial material properties of both processes. The results for different methanol concentrations fed to the PFC device, are presented in Figure 3.

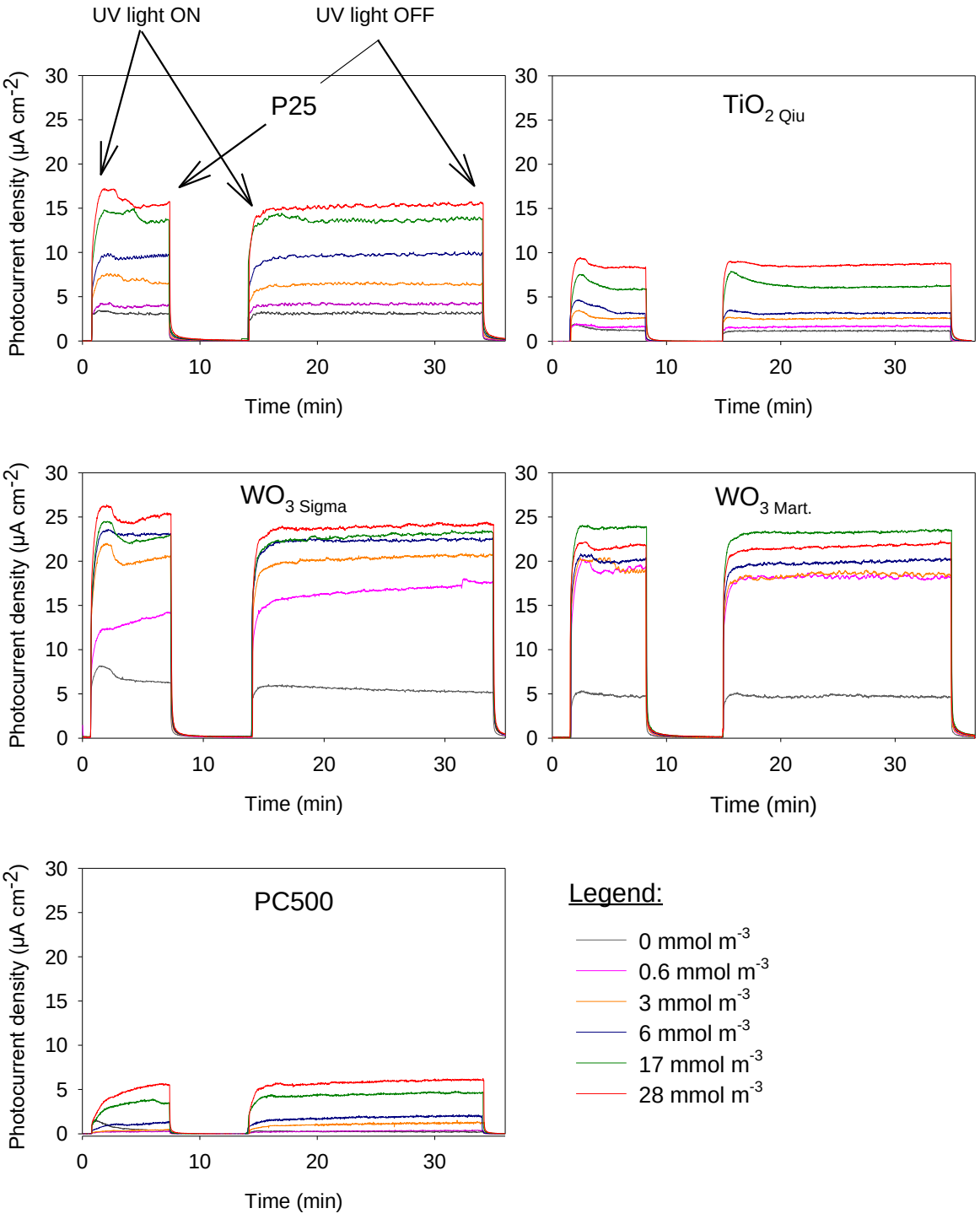

Figure 3. PFC: Photocurrent density as a function of time when feeding the photoanode with moist methanol vapours of different concentrations (see legend, expressed in millimoles of methanol m^{-3}) when using different photocatalysts at the photoanode.

The CA measurements, shown in Figure 3, show an increase in generated photocurrent for all studied photocatalysts when methanol vapour was introduced in the photoanode feed, in accordance to what

was observed by Kaneko and co-workers for aqueous methanol streams (only for TiO_2) [19]. A control experiment (MEA without photocatalyst) was performed, showing no increase in generated photocurrent upon UV illumination of the cell (Fig. S10). The increase in photocurrent upon methanol introduction can be explained by the lower oxidation potential of methanol compared to that of water (0.03 V *vs.* 1.23 V at pH 0 and *vs.* NHE, respectively) [31], which makes it a more efficient hole scavenger and results in less recombination losses. In addition, the current doubling effect is a well-known phenomenon related to increased photocurrent generation upon introduction of methanol. It is associated with the formation of intermediate radicals during oxidation of the hole scavenger, resulting in the injection of an electron into the conduction band of the photocatalyst, obtaining two electrons from one absorbed photon (one photogenerated and one injected) [10]. As expected, it can be observed that the increase in generated photocurrent upon methanol introduction is higher at higher methanol concentrations in the moist vapours (Figure 3). Also note that, overall, very stable photocurrents are obtained over time, highlighting the robustness of the system used in this study.

When considering the first 'light-ON' phase in Figure 3, a standard photocurrent profile can be observed, as described in detail by Rongé and co-workers, with an initial anodic overshoot, followed by a steady state current increase and eventually current decay until the light is turned off. The anodic overshoot is absent in almost all of the second 'Light ON' phases, due to repetition of the illumination [32]. The absence of the initial anodic spike for PC500 again reflects the poor electronic properties of this photocatalyst, as hole trapping by surface states at the photoanode surface is known as an important contributor to the generation of an anodic overshoot [33].

An important performance indicator for future application of gas phase PFC technology is the absolute photocurrent generation. For a pure water vapour feed, the highest photocurrents are obtained using both WO_3-based materials: $WO_{3\ Sigma}$ > $WO_{3\ Mart.}$ > P25 > $TiO_{2\ Qiu}$ > PC500. Additionally, strong increases in photocurrent are observed for these WO_3-based photocatalysts when adding methanol vapour to

the feed, outperforming the TiO_2-based photocatalysts over the full methanol concentration range. The higher absolute photocurrents generated using WO_3-based photocatalysts can be ascribed to the higher electron mobility of WO_3 (~ 5 $cm^2 V^{-1} s^{-1}$) compared to TiO_2 (~ 0.2 $cm^2 V^{-1} s^{-1}$) [34]. These results clearly highlight the importance of efficient electron transport in a PFC. To our knowledge, these are the first promising results for application of WO_3-based photocatalysts in a gas phase PFC system. A property known for influencing the electron mobility of a photocatalyst is its crystal structure [35], which is reflected in the results of the TiO_2-based photocatalysts. While both WO_3-based photocatalysts reach similar absolute photocurrents (both monoclinic crystal structures), distinct differences can be observed between the different TiO_2-based photocatalysts. Polycrystalline photocatalysts (in this case P25 and $TiO_{2\ Qiu}$, *cfr*. Supporting Information) are known for their higher electron mobility compared to single-crystal materials [35], such as PC500 (pure anatase). In addition, the ratio anatase/rutile of the commercially available P25 is close to optimal, while this is presumably not the case for $TiO_{2\ Qiu}$. PC500 is known to have very poor electronic properties, resulting in very low charge carrier stability [36], explaining the strikingly low absolute photocurrent generation observed for this photocatalyst and thus eliminating this photocatalyst for use in (unbiased) gas phase PFC's, while on the other hand it is known to be an excellent material in pure gas phase photocatalysis [37].

As the final goal is to obtain an autonomously operating sunlight-driven PFC device solely using polluted air to sustainably generate electricity, additional CA measurements using simulated solar light (and solely visible light) were performed as proof-of-concept and are shown in Figure 4 for P25 and $WO_{3\ Sigma}$ and in the Supporting Information section (Fig. S11) for the other photocatalysts. Autonomous un-biased performance of the PFC was obtained with all studied photocatalysts when feeding the PFC with methanol-rich vapours. These results also underline the suitability of WO_3 as photoanode for this application. The smaller band gap of WO_3 (Table 1) enables absorption of visible light besides UV light, thus working with (simulated) solar light instead of solely UV light results in the generation of higher absolute photocurrents and consequently an even higher photocurrent increase

compared to TiO_2-based photocatalysts. Note that the UV measurements were performed with a different lamp as the two other measurements (thus obtaining a different irradiance spectrum as can be seen in Fig. S4), and consequently the sum of the generated photocurrents obtained under visible and UV light does not equal the photocurrent generated under simulated solar light (AM1.5).

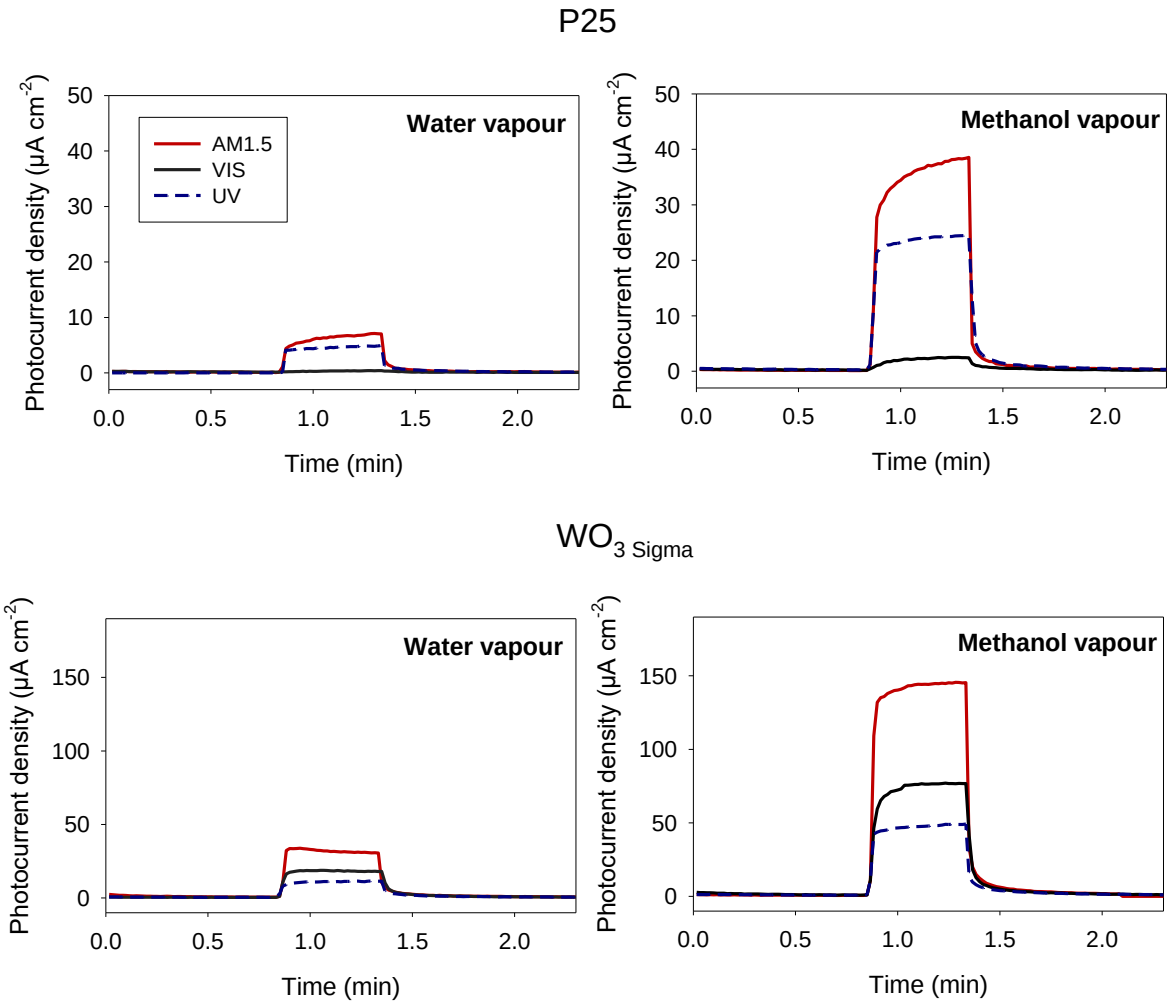

Figure 4. PFC – Solar light response: Photocurrent density as a function of time when using different light sources (simulated sunlight (AM1.5, 100 mW cm^{-2}), visible light (solar simulator with cut-on filter > 420 nm) and UV light (adjusted to 4 mW cm^{-2})), both when feeding the photoanode with pure water vapour and moist methanol vapour (17 mmol m^{-3}) when using P25 and $WO_{3\ Sigma}$ at the photoanode.

A clear difference in concentration response can be seen between the TiO_2 and WO_3-based photocatalysts (Figure 3 and Table 2). While both WO_3-based materials follow a similar trend, with a steep increase in generated photocurrent even for low methanol concentrations that levels off at higher methanol concentrations, $TiO_{2\ Qiu}$ and PC500 on the other hand show a distinct proportional increase in generated photocurrent over the entire concentration range, but without reaching the

absolute photocurrents generated by the WO_3-based photocatalysts. The concentration response of P25 follows a trend in-between. It is rationalized that decomposition of small quantities of methanol on WO_3 is already very efficient, resulting in only small photocurrent increases at higher methanol concentrations with the same amount of photocatalyst, especially considering the small surface area that eventually results in saturation or even a drop in photocurrent generation, as seen for $WO_{3\ Mart}$. Such a decrease in photocurrent upon increasing the concentration of an organic compound might also be ascribed to the formation of intermediates acting as recombination centres, as described by Xie and co-workers [18]. Due to the larger surface area of all TiO_2-based photocatalysts (Table 1) saturation of the surface at high methanol concentrations is less likely for these photoanodes, and proportionally increasing photocurrent generation with increasing methanol concentration is expected (Table 2), as long as surface saturation is avoided. In addition, the high relative increase in generated photocurrent density upon introduction of high methanol concentrations observed for PC500 might be due to a combination of the favourable morphological characteristics of PC500 and the fact that methanol acts as a hole scavenger that largely reduces recombination rate. It should be kept in mind though, that PC500 performs very poorly in absolute terms.

Table 2. Relative increase in generated photocurrent obtained with a moist methanol vapour relative to the photocurrent generated with pure water vapour ($I_{methanol}/I_{H2O}$).

	$I_{Methanol}$ / I_{H2O}				
Methanol conc. (mmol m^{-3})	**P25**	**$TiO_{2\ Qiu}$**	**$WO_{3\ Sigma}$**	**$WO_{3\ Mart.}$**	**PC500**
0.6	1.3	1.5	3.2	4.0	1.6
2.8	2.0	2.3	3.9	4.0	5.8
5.6	3.2	2.9	4.5	4.4	9.8
16.9	4.3	5.5	4.6	5.1	23.1
28.1	4.9	7.8	4.6	4.8	30.5

Interestingly, the photocatalysts resulting in the lowest direct photocatalytic methanol conversion (Figure 2), *i.e.* both types of WO_3, actually lead to the highest absolute photocurrent generation when applying the same methanol vapour concentration (28 mmol m^{-3}) to the photoanode feed (Figure 3). In terms of absolute photocurrent increase generated by adding 28 mmol m^{-3} methanol to the

photoanode, the following order can be obtained (expressed in µA cm^{-2}): $WO_{3\ Sigma}$ (18.6) > $WO_{3\ Mart.}$ (17.4) > P25 (12.2) > $TiO_{2\ Qiu}$ (7.5) > PC500 (5.9). Thus, a clear difference is observed in the performance of the different photocatalysts when comparing both air remediation technologies (photocatalysis *vs.* PFC). Although photocatalysis is the driving force behind the functional operation of a PFC, large differences are clearly induced by physically separating the ongoing reactions in two distinct compartments. Therefore, material properties that are beneficial for photocatalytic VOC degradation might be less crucial for photoelectrochemical VOC degradation and *vice versa*. For example, although the high surface area of the studied types of TiO_2 contributed to enhanced direct photocatalytic methanol conversion, this property clearly appears less important for photoelectrochemical VOC oxidation. Good electron mobility on the other hand proves crucial for an efficient PFC system, while of lesser importance for purely gas phase photocatalytic systems. This is clearly evidenced by the fact that the poor electronic properties of PC500 did not result in much lower photocatalytic methanol conversion compared to the other photocatalysts, but did largely decrease the absolute photocurrents that were obtained in the PFC.

In the next section, CV analysis contributes to the understanding of gas phase PFC operation. It should be stressed that this technique has only scarcely been applied in the field of gas phase PFC [38]. CV measurements were performed for all studied photocatalysts, both for pure water vapour and a moist methanol vapour (17 mmol m^{-3}) as photoanode feed. The results are shown in Figure 5. The initial CV measurements were performed between - 0.2 and 1 V.

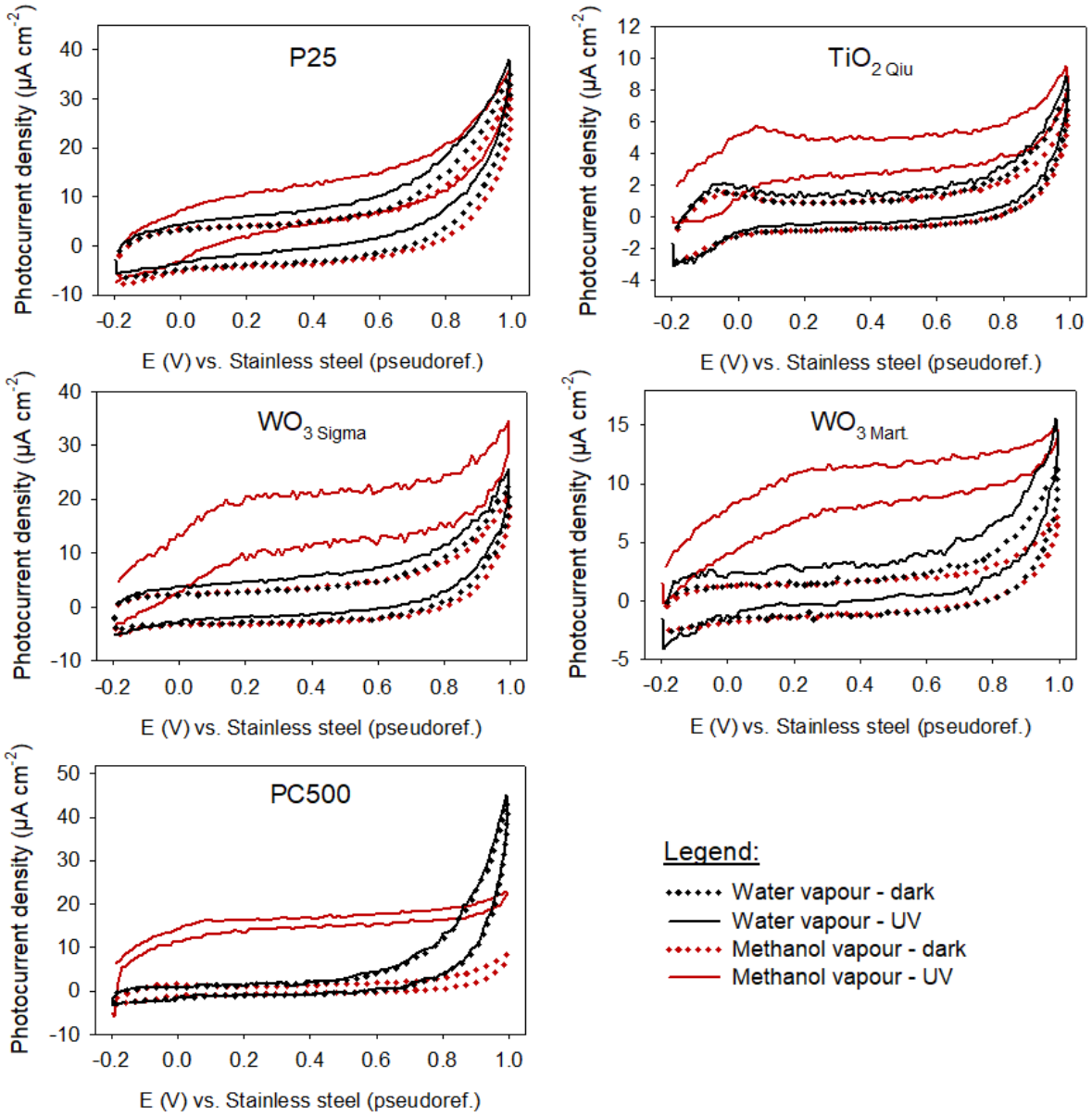

Figure 5. PFC: Cyclic voltammograms (scan rate = 10 mV s^{-1}) obtained for pure water vapour and moist methanol vapour (17 mmol m^{-3}), both in dark and under UV illumination when using different photocatalysts at the photoanode.

The results from Figure 5 confirm that upon illumination of the PFC whilst feeding the photoanode with pure water vapour, a small increase in generated current (the photocurrent) can be observed for all materials compared to dark conditions (almost not observable for PC500, which is in agreement with the CA measurements). When adding methanol vapour (17 mmol m^{-3}) to the photoanode feed in dark, no increase in generated current was observed. In fact, the voltammogram nicely coincides with that of pure water vapour for all photocatalysts except at high potentials where a small decrease in generated current can be observed upon introducing methanol. This might be attributed to the onset

of oxygen evolution at this potential, which shall be discussed later. When the PFC is illuminated whilst feeding with methanol vapour, a large increase in generated current can be observed for all studied photocatalysts compared to the dark result. As in the unbiased CA measurements, under illumination an increase in the absolute generated photocurrent is observed when methanol was added to pure water vapour at the photoanode. A control experiment (MEA without photocatalyst) was performed, showing no change in current upon introduction of either UV light or methanol vapour (Fig. S12), thus evidencing that the changes in generated photocurrent observed in Figure 5 are only due to photoelectrochemical reactions. The peak (*ca.* 0.06 V) derived for $TiO_{2\ Qiu}$ in the anodic scan obtained with moist methanol vapour cannot be attributed to methanol oxidation, as it is also observed when flushing with pure water vapour (*ca.* -0.04 V). EDXRF measurements (Supporting Information Fig. S7) showed no detectable impurities in the material (when compared to P25) that could explain this observation.

Although all studied photocatalysts show photoelectrochemical methanol oxidation, clear differences can be observed amongst the different materials (*e.g.* shape CV, absolute photocurrents). In order to determine the key performance indicators of the studied PFC systems, more extensive CV measurements were performed, scanning to higher (1.5 V) and lower (-1 V) applied potentials. The results for P25 and $WO_{3\ Sigma}$ are shown in Figure 6. The results obtained with $TiO_{2\ Qiu}$, $WO_{3\ Mart.}$ and PC500 are provided in the Supporting Information section (Fig. S13).

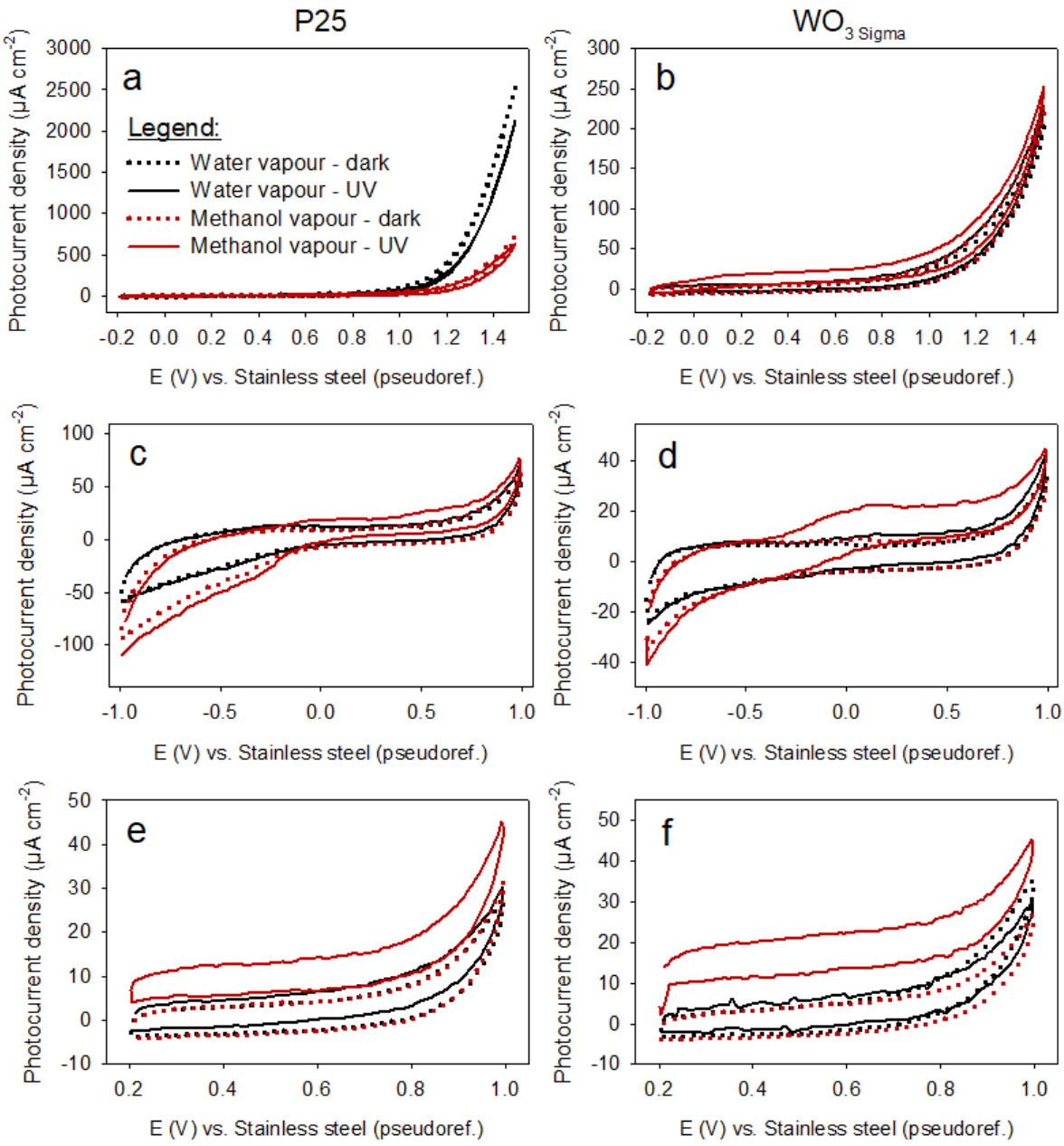

Figure 6. PFC: Cyclic voltammograms showing the effect of the applied potential window (scan rate = 10 mV s^{-1}) obtained for pure water vapour and moist methanol vapour (17 mmol m^{-3}), both in dark and under UV illumination when using (left) P25 and (right) $WO_{3\ Sigma}$ at the photoanode.

Figure 6a (CV till 1.5 V) shows that for P25 a steep increase in generated (photo)current is induced around 1.1 V both in dark and under UV, which is less pronounced when feeding the photoanode with a moist methanol vapour (*vs.* pure water vapour). This steep increase in generated current can be attributed to the onset of the oxygen evolution reaction (OER) [39]. When studying the CVs ranging till -1 V (Figure 6c/d and Fig. S13) a clear reaction can also be observed for all photocatalysts at very low

applied potentials. The observed decrease in generated current at these low (negative) potentials can be attributed to the onset of the hydrogen evolution reaction (HER) [40].

When analysing at the anodic curve of Figure 6c (CVs till -1 V) it can be observed for P25 that at -0.32 V the photocurrents (UV) generated when flushing with a moist methanol vapour no longer coincide with the currents obtained in dark, but are shifted upwards. This sudden upward photocurrent shift can be attributed to the onset of methanol oxidation. To further study this, an additional CV measurement was performed for all photocatalysts initiating the CV measurement at 0.2 V (incl. 5s equilibration at 0.2 V, Figure 6e/f and Fig. S13). In this measurement, it could be observed for all photocatalysts that the generated photocurrents obtained when the photoanode was fed with a moist methanol vapour (under UV illumination) were distinctly shifted upwards compared to the currents obtained in dark and with pure water vapour. This distinct upward shift started immediately at the initial applied potential. This indicates that the methanol molecules present in the vicinity of the electrode surface are already oxidised, *i.e.* oxidised at a potential below 0.2 V, hence the initial current is not zero. This distinct upward shift in photocurrent generation directly starting at 0.2 V was present for all studied photocatalysts.

In further characterisation of the PFC system, Table 3 summarises the efficiency parameters calculated from the CV measurements. The measured open-circuit voltages (V_{oc}) can be compared to the maximal theoretically expected V_{oc}. The V_{oc} can be regarded as the force driving the electron flow from photoanode to cathode during unbiased PFC operation and is thus determined by the difference between the energy level of the conduction band of the selected photocatalyst and the redox potential of the cathodic reaction. For the theoretical maximal V_{oc}, reduction towards H_2O is assumed at the cathode (1.23 V *vs.* NHE at pH=0), although H_2O_2 formation (0.68 V *vs.* NHE at pH=0) is also technically possible and often favoured due to its lower redox potential. Thus, depending on the exact reaction at the cathode, the measured V_{oc} can deviate largely from the theoretical maximum value. The ratio of the measured V_{oc} to the theoretical maximal V_{oc} was also used by Kaneko and co-workers as a rough

estimate for the fuel-to-electricity conversion [19], and is shown for all studied photocatalysts in Table 3 (= fuel-eff. (%)). The WO_3-based photocatalysts present the highest fuel-to-electricity conversion, associated with the highest V_{oc} values.

Table 3. Efficiency parameters of studied photocatalysts when working with a moist methanol feed (17 mmol m^{-3}).

	J_{sc} (µA cm^{-2})	V_{oc} (V)	P_{max} (µW cm^{-2})	Fuel-eff. (%)	η (%)	FF
P25	19.9	0.54	3.1	42	0.13	0.29
$TiO_{2\ Qiu}$	6.1	0.78	1.4	60	0.06	0.30
$WO_{3\ Sigma}$	19.4	0.83	4.4	70	0.19	0.27
$WO_{3\ Mart.}$	11.5	0.79	3.5	66	0.15	0.39
PC500	23.4	0.27	1.8	19	0.08	0.28

Polarisation curves (J-V plot), obtained as described by Antoniadou and co-workers [8] and added in the Supporting Information section (Fig. S14a), were used to obtain the real maximal electric power output $(J.V)_{max}$ or P_{max}. P_{max} can be used to determine the overall efficiency (η) by dividing P_{max} by the power density of the incident radiation (2.35 mW cm^{-2}). The highest η-values were also found for both WO_3-based photocatalysts, followed by P25, with very low values for both PC500 and $TiO_{2\ Qiu}$. The critical note should be added that the obtained η-values are still quite low, as this is the first study on the application of a PFC for gas phase VOC degradation. This study merely aims at showcasing the potential of this technique for the conversion of gaseous pollutants, such as VOCs, serving as fuel for sustainable electricity production. The next step will be to optimise the materials and the process as a whole. Still, the PFC process as used in this study already enables to convert large parts of the energy stored in the degraded VOC to electricity, with both WO_3-based photocatalysts exceeding 65% conversion.

The fill factor (FF) was calculated for all photocatalysts by dividing P_{max} by the theoretical maximal power output ($V_{oc}.J_{sc}$). The FFs obtained with both TiO_2 and WO_3-based photocatalysts are significantly higher than those obtained in liquid phase PFC systems working with a methanol solution as reported by Hu and co-workers, showing FFs of 0.17 and 0.11 for TiO_2 and WO_3, respectively [41], while FFs up to 0.39 are attained in our work. This can be attributed to the cell configuration used in this study

combining anode, electrolyte and cathode in a MEA, reducing electrolyte resistance and associated current losses due to the reduced distance between the two electrodes. In the study of Hu and co-workers the TiO_2-photoanode performed better than the WO_3 one [41]. Both the difference in cell configuration (reduced recombination and thus possibly benefiting WO_3), operating phase (drastically lower diffusion limitations could play an important role in gas phase operation, amongst others) and the different nature of the studied photocatalysts can contribute to this difference. For completeness, power density (J-P) curves can be found in the Supporting Information section (Fig. S14b).

To summarise, this study illustrates the potential of a PFC, using a WO_3-based photoanode, as waste-to-energy recovering air purification device. The described proof-of-concept can serve further development of an autonomous, low-cost and widely applicable gas phase PFC system.

4. Conclusion

In this study an autonomous, robust, low-cost, and widely applicable PFC device targeting air instead of water pollution was presented. Simultaneous waste gas degradation, using methanol as a model compound, and electricity production were achieved in the absence of an electrical bias. WO_3-based photocatalysts were successfully applied, for the first time, as photoanode material under these conditions. Improved insight into the driving material parameters behind gas phase photofuel cell operation was obtained by comparing direct photocatalytic and photoelectrochemical gas phase experiments for five different materials. The partially visible light-active WO_3 photoanodes clearly outperformed the UV-active TiO_2-based electrodes both under pure UV and solar light irradiation. They resulted in the highest steady state photocurrent, fuel-to-electricity conversion (> 65%) and overall efficiency, proving promising candidates as photoanodes for an autonomously operating sunlight-driven PFC device solely using polluted air to sustainably generate electricity. In contrast, both studied WO_3-based photocatalysts resulted in the lowest direct photocatalytic methanol conversion (~ 65%), highlighting the difference in driving material properties between both processes. While the low

surface area of both WO_3-based photocatalysts reduced the direct photocatalytic performance of these materials, this property seemed of lesser importance in a gas phase PFC, which on the other hand largely benefits from the high electron mobility provided by WO_3-based materials. This study aims to serve as proof-of-concept towards further development of an autonomous, low-cost and widely applicable waste gas-to-electricity PFC device.

Declaration of Competing Interests

The authors declare no competing interests.

Acknowledgements

M.V.H. acknowledges the Research Foundation–Flanders (FWO) for a doctoral fellowship (1135619N). R.C. acknowledges funding from the European Union's Horizon 2020 research and innovation programme under the Marie Skłodowska-Curie grant agreement No 842219.

References

[1] World Health Organisation, Ambient air pollution: a global assessment of exposure and burden of disease, 2016.

[2] S.W. Verbruggen, TiO2 photocatalysis for the degradation of pollutants in gas phase: From morphological design to plasmonic enhancement, J. Photochem. Photobiol. C Photochem. Rev. 24 (2015) 64–82. doi:10.1016/j.jphotochemrev.2015.07.001.

[3] N. Blommaerts, R. Asapu, N. Claes, S. Bals, S. Lenaerts, S.W. Verbruggen, Gas phase photocatalytic spiral reactor for fast and efficient pollutant degradation, Chem. Eng. J. 316 (2017) 850–856. doi:10.1016/j.cej.2017.02.038.

[4] B.D. Boruah, A. Mathieson, B. Wen, C. Jo, F. Deschler, M. De Volder, Photo-Rechargeable Zinc-Ion Capacitor Using 2D Graphitic Carbon Nitride, Nano Lett. 20 (2020) 5967–5974. doi:10.1021/acs.nanolett.0c01958.

[5] D.H. Guan, X.X. Wang, M.L. Li, F. Li, L.J. Zheng, X.L. Huang, J.J. Xu, Light/Electricity Energy Conversion and Storage for a Hierarchical Porous In2S3@CNT/SS Cathode towards a Flexible Li-CO2 Battery, Angew. Chemie - Int. Ed. 59 (2020) 19518–19524. doi:10.1002/anie.202005053.

[6] L. Bai, H. Huang, S. Zhang, L. Hao, Z. Zhang, H. Li, L. Sun, L. Guo, H. Huang, Y. Zhang, Photocatalysis-Assisted Co3O4/g-C3N4 p–n Junction All-Solid-State Supercapacitors: A Bridge between Energy Storage and Photocatalysis, Adv. Sci. 7 (2020) 1–9. doi:10.1002/advs.202001939.

[7] M. Antoniadou, P. Lianos, Photoelectrochemical oxidation of organic substances over nanocrystalline titania: Optimization of the photoelectrochemical cell, Catal. Today. 144 (2009)

166–171. doi:10.1016/j.cattod.2009.02.024.
[8] M. Antoniadou, P. Bouras, N. Strataki, P. Lianos, Hydrogen and electricity generation by photoelectrochemical decomposition of ethanol over nanocrystalline titania, Int. J. Hydrogen Energy. 33 (2008) 5045–5051. doi:10.1016/j.ijhydene.2008.07.005.
[9] P. Lianos, N. Strataki, M. Antoniadou, Photocatalytic and photoelectrochemical hydrogen production by photodegradation of organic substances, Pure Appl. Chem. 81 (2009) 1441–1448. doi:Doi 10.1351/Pac-Con-08-07-07.
[10] M. Antoniadou, P. Lianos, Production of electricity by photoelectrochemical oxidation of ethanol in a PhotoFuelCell, Appl. Catal. B Environ. 99 (2010) 307–313. doi:10.1016/j.apcatb.2010.06.037.
[11] M. Antoniadou, D.I. Kondarides, P. Lianos, Photooxidation products of ethanol during photoelectrochemical operation using a nanocrystalline titania anode and a two compartment chemically biased cell, Catal. Letters. 129 (2009) 344–349. doi:10.1007/s10562-009-9863-8.
[12] B. Seger, G.Q. (Max) Lu, L. Wang, Electrical power and hydrogen production from a photo-fuel cell using formic acid and other single-carbon organics, J. Mater. Chem. 22 (2012) 10709. doi:10.1039/c2jm16635f.
[13] J. Rongé, S. Deng, S. Pulinthanathu Sree, T. Bosserez, S.W. Verbruggen, N. Kumar Singh, J. Dendooven, M.B.J. Roeffaers, F. Taulelle, M. De Volder, C. Detavernier, J. a. Martens, Air-based photoelectrochemical cell capturing water molecules from ambient air for hydrogen production, RSC Adv. 4 (2014) 29286. doi:10.1039/C4RA05371K.
[14] J. Georgieva, S. Armyanov, I. Poulios, S. Sotiropoulos, An all-solid photoelectrochemical cell for the photooxidation of organic vapours under ultraviolet and visible light illumination, Electrochem. Commun. 11 (2009) 1643–1646. doi:10.1016/j.elecom.2009.06.019.
[15] J. Georgieva, S. Armyanov, I. Poulios, a. D. Jannakoudakis, S. Sotiropoulos, Gas Phase Photoelectrochemistry in a Polymer Electrolyte Cell with a Titanium Dioxide/Carbon/Nafion Photoanode, Electrochem. Solid-State Lett. 13 (2010) 11–13. doi:10.1149/1.3465306.
[16] J. Georgieva, TiO2/WO3 photoanodes with enhanced photocatalytic activity for air treatment in a polymer electrolyte cell, J. Solid State Electrochem. 16 (2012) 1111–1119. doi:10.1007/s10008-011-1504-7.
[17] S.W. Verbruggen, M. Van Hal, T. Bosserez, J. Rongé, B. Hauchecorne, J.A. Martens, S. Lenaerts, Harvesting hydrogen gas from air pollutants with an un-biased gas phase photo-electrochemical cell, ChemSusChem. 10 (2017) 1413–1418. doi:10.1002/cssc.201601806.
[18] S. Xie, K. Ouyang, Degradation of refractory organic compounds by photocatalytic fuel cell with solar responsive WO3/FTO photoanode and air-breathing cathode, J. Colloid Interface Sci. 500 (2017) 220–227. doi:10.1016/j.jcis.2017.04.002.
[19] M. Kaneko, J. Nemoto, H. Ueno, N. Gokan, K. Ohnuki, M. Horikawa, R. Saito, T. Shibata, Photoelectrochemical reaction of biomass and bio-related compounds with nanoporous TiO2 film photoanode and O2-reducing cathode, Electrochem. Commun. 8 (2006) 336–340. doi:10.1016/j.elecom.2005.12.004.
[20] Z. Yang, M. Zhu, Y. Niu, E. Kozliak, B. Yao, Y. Zhang, C. Zhang, T. Qin, Y. Jia, Q. Li, A Graphene-Based Coaxial Fibrous Photofuel Cell Powered by Mine Gas, Adv. Funct. Mater. 29 (2019). doi:10.1002/adfm.201906813.
[21] B. Seger, P. V. Kamat, Fuel cell geared in reverse: Photocatalytic hydrogen production using a TiO2/Nafion/Pt membrane assembly with no applied bias, J. Phys. Chem. C. 113 (2009) 18946–18952. doi:10.1021/jp907367k.
[22] S. Qiu, S.J. Kalita, Synthesis, processing and characterization of nanocrystalline titanium dioxide, Mater. Sci. Eng. A. 435–436 (2006) 327–332. doi:10.1016/j.msea.2006.07.062.
[23] D.S. Martínez, E.L. Cuéllar, Synthesis and characterization of WO3 nanoparticles prepared by the precipitation method: Evaluation of photocatalytic activity under vis-irradiation, Solid State Sci. 12 (2010) 88–94. doi:10.1016/j.solidstatesciences.2009.10.010.
[24] S.W. Verbruggen, S. Deng, M. Kurttepeli, D.J. Cott, P.M. Vereecken, S. Bals, J.A. Martens, C. Detavernier, S. Lenaerts, Photocatalytic acetaldehyde oxidation in air using spacious TiO2films

prepared by atomic layer deposition on supported carbonaceous sacrificial templates, Appl. Catal. B Environ. 160–161 (2014) 204–210. doi:10.1016/j.apcatb.2014.05.029.
[25] D. Sanchez-Martinez, A. Martinez-De La Cruz, E. Lopez-Cuellar, Synthesis of WO3 nanoparticles by citric acid-assisted precipitation and evaluation of their photocatalytic properties, Mater. Res. Bull. 48 (2013) 691–697. doi:10.1016/j.materresbull.2012.11.024.
[26] M. Nuno, R.J. Ball, C.R. Bowen, Photocatalytic Properties of Commercially Available TiO2 Powders for Pollution Control, in: Semicond. Photocatal. - Mater. Mech. Appl. Anatase, 2016: pp. 614–634. doi:http://dx.doi.org/10.5772/57353.
[27] X. Deng, Y. Yue, Z. Gao, Gas-phase photo-oxidation of organic compounds over nanosized TiO2 photocatalysts by various preparations, Appl. Catal. B Environ. 39 (2002) 135–147. doi:10.1016/S0926-3373(02)00080-2.
[28] C. Günnemann, C. Haisch, M. Fleisch, J. Schneider, A. V. Emeline, D.W. Bahnemann, Insights into Different Photocatalytic Oxidation Activities of Anatase, Brookite, and Rutile Single-Crystal Facets, ACS Catal. 9 (2019) 1001–1012. doi:10.1021/acscatal.8b04115.
[29] T. Ohno, K. Sarukawa, K. Tokieda, M. Matsumura, Morphology of a TiO2 photocatalyst (Degussa, P-25) consisting of anatase and rutile crystalline phases, J. Catal. 203 (2001) 82–86. doi:10.1006/jcat.2001.3316.
[30] S.Y. Toledo Camacho, A. Rey, M.D. Hernández-Alonso, J. Llorca, F. Medina, S. Contreras, Pd/TiO2 -WO3 photocatalysts for hydrogen generation from water-methanol mixtures, Appl. Surf. Sci. 455 (2018) 570–580. doi:10.1016/j.apsusc.2018.05.122.
[31] W. Zhang, Y. Hu, L. Ma, G. Zhu, Y. Wang, X. Xue, R. Chen, S. Yang, Z. Jin, Progress and Perspective of Electrocatalytic CO2 Reduction for Renewable Carbonaceous Fuels and Chemicals, Adv. Sci. 5 (2018). doi:10.1002/advs.201700275.
[32] J. Rongé, D. Nijs, S. Kerkhofs, K. Masschaele, J. a Martens, Chronoamperometric study of membrane electrode assembly operation in continuous flow photoelectrochemical water splitting., Phys. Chem. Chem. Phys. 15 (2013) 9315–25. doi:10.1039/c3cp50890k.
[33] S.W. Verbruggen, J.J.J. Dirckx, J.A. Martens, S. Lenaerts, Surface photovoltage measurements: A quick assessment of the photocatalytic activity?, Catal. Today. 209 (2013) 215–220. doi:10.1016/j.cattod.2012.11.010.
[34] Y. Liu, C. Xie, J. Li, T. Zou, D. Zeng, New insights into the relationship between photocatalytic activity and photocurrent of TiO2/WO3 nanocomposite, Appl. Catal. A Gen. 433–434 (2012) 81–87. doi:10.1016/j.apcata.2012.05.001.
[35] T. Bak, M.K. Nowotny, L.R. Sheppard, J. Nowotny, Mobility of electronic charge carriers in titanium dioxide, J. Phys. Chem. C. 112 (2008) 12981–12987. doi:10.1021/jp801028j.
[36] M. Keulemans, S.W. Verbruggen, B. Hauchecorne, J.A. Martens, S. Lenaerts, Activity versus selectivity in photocatalysis: Morphological or electronic properties tipping the scale, J. Catal. 344 (2016) 221–228. doi:10.1016/j.jcat.2016.09.033.
[37] S.W. Verbruggen, K. Masschaele, E. Moortgat, T.E. Korany, B. Hauchecorne, J.A. Martens, S. Lenaerts, Factors driving the activity of commercial titanium dioxide powders towards gas phase photocatalytic oxidation of acetaldehyde, Catal. Sci. Technol. 2 (2012) 2311–2318. doi:10.1039/c2cy20123b.
[38] Z. Yang, M. Zhu, Y. Niu, E. Kozliak, B. Yao, Y. Zhang, C. Zhang, T. Qin, Y. Jia, Q. Li, A Graphene-Based Coaxial Fibrous Photofuel Cell Powered by Mine Gas, Adv. Funct. Mater. 29 (2019) 1–8. doi:10.1002/adfm.201906813.
[39] C.A. Martinez-Huitle, M.A. Rodrigo, O. Scialdone, Electrochemical water and Wastewater Treatment, Elsevier Inc., 2018. doi:10.4135/9781452240084.n240.
[40] N. Dubouis, A. Grimaud, The hydrogen evolution reaction: From material to interfacial descriptors, Chem. Sci. 10 (2019) 9165–9181. doi:10.1039/c9sc03831k.
[41] C. Hu, D. Kelm, M. Schreiner, T. Wollborn, L. Mädler, W.Y. Teoh, Designing Photoelectrodes for Photocatalytic Fuel Cells and Elucidating the Effects of Organic Substrates, ChemSusChem. 8 (2015) 4005–4015. doi:10.1002/cssc.201500793.